Nonlinear Incremental Robust Model Predictive Control for a Nonlinear Aeroservoelastic System

Zhang, T.; Wang, Xuerui

Important note
To cite this publication, please use the final published version (if applicable).
Please check the document version above.

NONLINEAR INCREMENTAL ROBUST MODEL PREDICTIVE CONTROL FOR A NONLINEAR AEROSERVOELASTIC SYSTEM

Tingyu Zhang[1] **and Xuerui Wang**[2]

[1]Delft University of Technology
Kluyverweg 1, 2629HS Delft, The Netherlands
T.Zhang-6@tudelft.nl

[2]Delft University of Technology
Kluyverweg 1, 2629HS Delft, The Netherlands
X.Wang-6@tudelft.nl

Keywords: robust nonlinear model predictive control, incremental nonlinear dynamic inversion, limit cycle oscillation

Abstract: This paper presents a novel approach to suppress gust-induced limit cycle oscillations (LCOs). The proposed method integrates incremental nonlinear dynamic inversion (INDI) and robust nonlinear model predictive control (NMPC) with tightened constraints. The INDI method estimates and actively rejects gusts, resulting in a reduced disturbance residue. The upper bound of the disturbance residue can be estimated either online or offline and is used to bound the maximum state deviation caused by uncompensated disturbances, thereby imposing tightened constraints for the NMPC scheme to improve the robustness of constraint satisfaction and stabilize the system. Simulation results on a 2-D nonlinear aeroservoelastic wing demonstrate that the proposed method stabilizes the nonlinear system and reduces the disturbed peak plunge and pitch motions by up to 20.69% and 33.70%, respectively. Additionally, the method mitigates the conservativeness of the robust NMPC, with an 81.67% reduction in the offline estimated upper bound of the disturbance residue. The online estimation of the disturbance residue captures its peak value while further relaxing the tightened constraint set when disturbance effects are small. The proposed control scheme effectively suppresses gust-induced LCO motions and reduces the conservativeness of the tightened constraint sets used in the robust NMPC [1].

1 INTRODUCTION

The development of next-generation civil aircraft has focused on weight savings through the use of lightweight materials and more aerodynamically efficient wings. These innovations have led to flexible wing designs, significantly increasing the nonlinear couplings between wing aerodynamics, inertia, and aeroservoelasticity. Consequently, nonlinear flexible wings are more sensitive to gusts and exhibit unstable and marginal stable phenomena, such as flutter and limit cycle oscillations (LCOs). Therefore, increasing attention has been given to gust disturbance rejection and nonlinear system stabilization through control means.

The dominant methods for rejecting gusts on flexible wings focus on controller synthesis using a linearized model trimmed at the cruise condition. Techniques such as static output feedback [2], linear quadratic regulator (LQR) [3], and linear quadratic Gaussian (LQG) [4–7] have demonstrated effective gust load alleviation (GLA) results on the linearized model in simulations. Multi-objective optimal controllers based on LQG and output feedback were proposed

in [8], which consider drag optimization, maneuver load alleviation, GLA, and flutter suppression in one controller synthesis. However, when these controllers are applied to the nonlinear model, degradations in controller performance are observed [6, 7]. To have the robustness of the controller against model uncertainties and external disturbances addressed, methods like $\mathcal{H}_\infty$ and μ synthesis [9] were developed for GLA on flexible wings equipped with Lidar, showing up to 72% peak bending moment reductions in simulations. Additionally, $\mathcal{H}_\infty$ with feedforward control [10] and $\mathcal{H}_\infty$ with observer-based active feedback control [11] further improved GLA results. These linear control methods have also been designed for active flutter suppression (AFS) tasks. A mixed $\mathcal{H}_2/\mathcal{H}_\infty$ gain scheduling control scheme [12] and a linear parameter-varying gain scheduled controller [13] were proposed to stabilize the nonlinear aeroservoelastic system. Closed-loop stability, robustness and disturbance rejection performances were shown through simulation. However, none of these linear control methods guarantee the nominal stability for nonlinear systems.

Research on controller design for disturbance rejection and stabilization directly on nonlinear flexible wings is limited, with few studies exploring incremental nonlinear dynamic inversion (INDI) [14, 15], nonlinear model predictive control (NMPC) [16–18], intelligent critic control [19], end-to-end deep reinforcement learning [20], and nonlinear distributed hamiltonian control [21]. Each of these approaches has its limitations: INDI does not address state constraints, NMPC requires the prediction of future gusts if the gust dynamics are embedded in the nominal system, the trained parameters in learning-based controllers lack physical insights, and nonlinear distributed Hamiltonian control from [21] requires an overhead gust sensor and a predefined gust model to predict gust propagation.

We aim to develop a method that enhances robustness against gusts and stabilizes the nonlinear system while maintaining all states within a safe operation range. There is a gap in control of the nonlinear flexible wing, as no current method addresses gust compensation using active disturbance rejection control, stabilization of the nonlinear system, and robust constraint satisfaction at once.

In control aspects, robust NMPC with tightened constraints [1] can achieve the desired stability and robust constraint satisfaction but tends to be overly conservative. Existing relaxation methods, such as sliding mode coupled robust NMPC [22], are complex when designing the sliding surface and suffer from chattering problems. Disturbance observer (DO) based robust NMPC [23] requires an estimated disturbance model, which is not always available. Hence, there is a need for a simpler method to reduce conservativeness in robust NMPC.

A loosely coupled INDI with NMPC for quadrotor control was proposed in [24], which used INDI for disturbance compensation and NMPC to provide virtual commands, demonstrating improved trajectory tracking ability under external disturbances compared to a differential flatness-based controller. However, state constraints are not considered explicitly, and the disturbed states may leave the safety bound. Inspired by this work, we develop an INDI-coupled robust NMPC to suppress the gust-induced LCOs. Our contributions include the following: Firstly, INDI compensates for part of the disturbances, resulting in a smaller disturbance residue. Secondly, the disturbance residue has a smaller upper bound than the nominal disturbance, allowing for less conservative tightened constraints used in the robust NMPC to stabilize the system. Moreover, we demonstrate that the upper bound of the disturbance residue can be estimated online, further relaxing the tightened constraints when the gust effects are small. Overall, the proposed method actively rejects disturbances, suppresses gust-induced LCOs, en-

hances robust constraint satisfaction, and reduces the conservativeness of the robust NMPC.

The rest of the paper is structured as follows. Section 2 presents a 2-D nonlinear aeroservoelastic system and background on the robust NMPC with tightened constraints. The control algorithm is derived in Section section 3, and modifications are made in Section 4 for a 2-D aeroservoelastic system. The proposed INDI-coupled robust NMPC is simulated in Section 5 and compared with nominal NMPC and robust NMPC. Conclusions are drawn in Section 6.

2 PRELIMINARIES

2.1 The aeroservoelastic model

The two-dimensional nonlinear aeroservoelastic model used in this study is taken from [19]:

$$
\begin{bmatrix} m_t & m_w x_\alpha b \\ m_w x_\alpha b & I_\alpha \end{bmatrix} \begin{bmatrix} \ddot{h} \\ \ddot{\alpha} \end{bmatrix} + \begin{bmatrix} c_h & 0 \\ 0 & c_\alpha \end{bmatrix} \begin{bmatrix} \dot{h} \\ \dot{\alpha} \end{bmatrix} \\
+ \begin{bmatrix} k_h(h) & 0 \\ 0 & k_\alpha(\alpha) \end{bmatrix} \begin{bmatrix} h \\ \alpha \end{bmatrix} = \begin{bmatrix} -L(\dot{h}, \alpha, \dot{\alpha}, \beta) \\ M(\dot{h}, \alpha, \dot{\alpha}, \beta) \end{bmatrix}
\tag{1}
$$

where h and α are the plunge displacement and the pitch angle. The model includes nonlinear stiffness parameters, $k_h(h)$ in a second-order polynomial form and $k_\alpha(\alpha)$ in a fourth order polynomial form, listed in (2) and (3). The inertia matrix contains parameters including the total mass m_t, the mass of the wing m_w, the moment of inertia I_α, the nondimensional distance from the elastic axis to the center of mass x_α, and the wing semi-chord length b. Additionally, the damping of the plunge and pitch motions are denoted as c_h and c_α. The aerodynamic force $L(\dot{h}, \alpha, \dot{\alpha}, \beta)$ and moment $M(\dot{h}, \alpha, \dot{\alpha}, \beta)$ are linear functions with respect to the surface deflection β.

$$
K_h = 2844(1 + 0.9h^2)
\tag{2}
$$

$$
K_\alpha = 2.82(1 - 22.1\alpha + 1315.5\alpha^2 - 8580\alpha^3 + 17289.7\alpha^4)
\tag{3}
$$

In addition to the aeroservoelastic model, the actuator dynamics is modeled as a first-order system with a cutoff frequency of 60 rad/s.

$$
\dot{\beta} + \omega_c \beta = \omega_c \beta_c
\tag{4}
$$

The input for the actuator is β_c. When combining the aeroservoelastic model and the actuator dynamics, we obtain the state vector $\begin{bmatrix} h & \alpha & \dot{h} & \dot{\alpha} & \beta \end{bmatrix}^T$ and a control input β_c. It is important to note that the given model represents a 2-D wing section. In real flight, the wing root and tip displacement will vary significantly. As the author of [19] does not specify the location of this wing section, the state constraint will only apply to the pitch angle, which ranges from -20 degrees to 20 degrees. Meanwhile, the surface deflection is limited between -10 to 10 degrees.

The considered perturbation, g_w, is the vertical 1-cos discrete-time wind gust with respect to the wing body frame. The disturbed pitch angle α_w has the form

$$
\alpha_w = \mathrm{atan}\left(\frac{U\sin\alpha - g_w}{U\cos\alpha}\right)
\tag{5}
$$

where $U = 15\ m/s$ is the free stream velocity. When the gust is presented, the α variable in the pitch stiffness coefficient k_α, lift L, and moment M is replaced by α_w. The state vector, the derivative of the state vector and the actual flap deflection are assumed to be continuous. Therefore, all perturbations can be treated as additive disturbances for the controller design.

2.2 Robust NMPC with tightened constraints

The model stated in (1) fits the criterion of an input affine nonlinear system described in (6):

$$\dot{x} = f(x) + g(x)u + w \tag{6}$$

where $x \in \mathbb{R}^n$ is the state vector, $u \in \mathbb{R}^p$ is the input vector, $n \geq p$, w is the additive disturbance, $f : \mathbb{R}^n \to \mathbb{R}^n$ and $g : \mathbb{R}^p \to \mathbb{R}^n$. The disturbance is assumed to be bounded, $||\omega|| \leq \bar{\omega}_m$, and x and u are constrained by subspaces $\mathbb{X} \in \mathbb{R}^n$ and $\mathbb{U} \in \mathbb{R}^p$.

Assumption 1 (Lipschitz continuous in $\bar{x}$) Let the nominal dynamics be $\dot{\bar{x}} = f(\bar{x}) + g(\bar{x})u$. There exists a Lipschitz constant $l > 0$, such that for any $\bar{x}_1, \bar{x}_2 \in \mathbb{R}^n$ and any $u \in \mathbb{R}^p$, $||f(\bar{x}_1) + g(\bar{x}_1)u - f(\bar{x}_2) - g(\bar{x}_2)u|| \leq l||\bar{x}_1 - \bar{x}_2||$. For a vector x, $||x||_Q = \sqrt{x^T Q x}$.

Assumption 1 states that the nominal model dynamics is Lipschitz continuous. This assumption is commonly seen in many input-affine nonlinear systems and is crucial for robustness analysis. Based on Assumption 1, with the same initial conditions and control input sequence starting at time t_0, the deviation between the nominal states $\bar{x}^*(t|t_0)$ and real states $x(t)$ is norm-bounded by (7) [1].

$$||\bar{x}^*(t) - x(t)|| \leq \frac{\bar{\omega}_m}{l}(e^{l(t-t_0)} - 1), \tag{7}$$

Equation 7 and its variations have appeared in many robust NMPC schemes [1, 22, 23] to describe the upper bound of the error between x and $\bar{x}^*$. Subsequently, robust NMPC with tightened constraints is designed as follows:

$$
\begin{aligned}
\mathbf{u}_{\text{opt}}(x) = &\underset{u}{\arg\min} \sum_{i=0}^{N-1} (||\bar{x}_i - x_{i,r}||_{Q_x} + ||u_i - u_{i,r}||_{Q_u}) + ||\bar{x}_N - x_{N,r}||_{Q_N} \\
&\text{subject to } \dot{\bar{x}}(t) = f(\bar{x}(t)) + g(\bar{x}(t))u(\bar{x}(t)), \\
&\bar{x}_i \in \mathbb{X} \sim \mathcal{B}_x(i), \ u_i \in \mathbb{U}
\end{aligned}
\tag{8}
$$

where the optimal control actions are derived by minimizing a discrete-time cost function with weighting matrices Q_x, Q_u and Q_N. The states and inputs are sampled in N equal time intervals spanning the prediction horizon T to perform numerical optimization. The operator $\sim$ is the Pontryagin set difference, i.e., given two sets $A \subseteq \mathbb{R}^n$ and $B \subseteq \mathbb{R}^n$, $A \sim B \triangleq \{z \in \mathbb{R}^n | z + y \in A, y \in B\}$. The set $\mathcal{B}_x(i)$ holds the upper bound on the sampled state deviation given by (9).

$$\mathcal{B}_x(i) = \{x \in \mathbb{R}^n | ||x|| \leq \frac{\bar{\omega}_m}{l}(e^{l\frac{T}{N}i} - 1)\}, \tag{9}$$

Consequently, the real states will satisfy the nominal constraints because the nominal states are forced to be bounded by the tightened constraint, $\bar{x}_i \in \mathbb{X} \sim \mathcal{B}_x(i)$, as described by (7). However, the time-related exponential term in (7) could render a small or even infeasible tightened constraint set, eventually leading to an unsolvable optimal control problem.

Previous works [22, 23] have used model-based active disturbance rejection techniques to alleviate the conservativeness of robust NMPC. Instead of maximum nominal disturbance, the

maximum disturbance residue is used to bound the state deviation. However, offline computation is still required to obtain the disturbance residue bound. The complexity of the controller design also increases due to the model-based active approach.

In the proposed approach, conservativeness is relaxed with a sensor-based INDI approach. A simple, computationally efficient online INDI-based method is proposed for the maximum possible state deviation estimation and disturbance rejection. Additionally, predefined margins for the tightened constraints and soft state constraints with slack variables are used to relax solver infeasibility problems when tightened constraints are infeasible and when the states are outside the tightened constraints. These state constraint margins are inspired by the methodology described in [16], where the authors considered future gusts linearly decreasing to zero over the first half of the prediction steps and assumed zero gusts for the latter half in their NMPC controller scheme. Setting margins on the tightened constraints implies that future disturbances will not exacerbate. This is a reasonable assumption since only the first control actions from NMPC are used. Additionally, the initial states are updated using the real state measurements at each controller sampling time, diminishing the significance of predictions beyond the first step.

3 METHODOLOGY

The control objectives of this study are active disturbance rejection and steering the states to the origin while adhering to input and state constraints. To achieve these objectives, an INDI-coupled robust NMPC with online maximum state deviation estimation is proposed. This controller integrates the optimal control action u_0^* with a disturbance compensation auxiliary controller u_{INDI}. The command input u_c is computed using (10):

$$u_c = u_0^* + u_{\text{INDI}}. \tag{10}$$

3.1 Disturbance estimation and rejection using INDI

This section introduces INDI-based control to estimate and actively reject disturbances. For systems in (6), the instantaneous additive disturbances can be estimated using the inverse of the dynamics and low-pass filtered state measurements, x_f, [24].

$$\omega = \dot{x}_f - f(x_f) - g(x_f)u_f \tag{11}$$

Equation 11 holds under the assumption that disturbances are slow-varying relative to the low-pass filtered dynamics. With the optimal control action u_0^*, the desired state derivative $\dot{x}_d$ is given by

$$\dot{x}_d = f(x_f) + g(x_f)u_0^*. \tag{12}$$

Subsequently, by substituting the estimated disturbances from (11) back into the system in (6), and replacing $\dot{x}$ with $\dot{x}_d$ from (12), an incremental expression for the command input is obtained in (13) where † is the pseudoinverse operator.

$$u_c = g(x_f)^\dagger(g(x_f)u_0^* - (\dot{x}_f - f(x_f) - g(x_f)u_f)) = u_0^* + u_{\text{INDI}} \tag{13}$$

Due to underactuation and input saturation, only a portion of the estimated disturbance is rejected. The remaining disturbance, or the disturbance residue, is used within the robust NMPC framework to estimate the state deviations.

3.2 Coupling INDI with robust NMPC

Upon solving the optimal control problem defined in (8), the optimal control action, u_0^*, for the first time step is extracted from $\mathbf{u}_{\text{opt}}$. The disturbance residue ω_{res} is then calculated using (14)

$$\omega_{\text{res}}(s) = \omega(s) + g(x_f(s))u_c - g(x_f(s))u_0^*, \tag{14}$$

where u_c and ω are from (13) and (11). The upper bound of the disturbance residue for traditional robust NMPC is defined by

$$\bar{\omega}_{m,\text{INDI}} = \sup_{s \in [0,\infty]} \omega_{\text{res}}(s) \leq \bar{\omega}_m, \tag{15}$$

with an offline parameter identification to find the minimal value of $\bar{\omega}_{m,\text{INDI}}$ through an infinite time span.

Due to the INDI disturbance compensation, this upper bound of disturbance residue is smaller than the nominal disturbance upper bound, resulting in a smaller upper bound on the state deviation. However, the upper bound from (15) can still have a large magnitude and lead to conservative tightened constraints, which will be demonstrated in simulations. To further relax the tightened constraints, a margin on the state constraint for future predictions is set, guaranteeing that the tightened constraints are feasible.

$$\bar{\omega}_{m,\text{INDI}}(t) = \sup_{s \in [t-t_s,t]} \omega_{\text{res}}(s). \tag{16}$$

Additionally, a sliding window online estimation of $\bar{\omega}_{m,\text{INDI}}$ with a window length of t_s is proposed to avoid the need for prior knowledge on $\bar{\omega}_m$ offline.

4 CASE STUDY ON THE 2-D NONLINEAR AEROSERVOELASTIC MODEL

The additive disturbance equivalent aeroservoelastic system, without considering the actuator dynamics, has state $\mathbf{x} = \begin{bmatrix} x_1 & x_2 & x_3 & x_4 \end{bmatrix}^T = \begin{bmatrix} h & \alpha & \dot{h} & \dot{\alpha} \end{bmatrix}^T$ and input $u = \beta$. Its dynamics can be expressed as

$$\dot{\mathbf{x}} = \begin{bmatrix} \dot{x}_1 \\ \dot{x}_2 \\ \dot{x}_3 \\ \dot{x}_4 \end{bmatrix} = f_{\text{ae}}(\mathbf{x}, u_{,h}, \omega_\alpha) = \begin{bmatrix} x_3 \\ x_4 \\ f_{\ddot{h}}(\mathbf{x}) + g_{\ddot{h}}(\mathbf{x})u + \omega_h \\ f_{\ddot{\alpha}}(\mathbf{x}) + g_{\ddot{\alpha}}(\mathbf{x})u + \omega_\alpha \end{bmatrix}, \tag{17}$$

with bounded additive disturbances ω_h and ω_α. The nominal system is represented by $\dot{\bar{\mathbf{x}}} = f_{\text{ae}}(\bar{\mathbf{x}}, u)$. The local Lipschitz assumption for this nominal system is given by

$$\begin{aligned}
&\|\ddot{\bar{\alpha}}_1(\bar{\mathbf{x}}_1, u) - \ddot{\bar{\alpha}}_2(\bar{\mathbf{x}}_2, u)\| \\
&= \| \begin{bmatrix} 0 & 0 & 0 & 1 \end{bmatrix} (f_{\text{ae}}(\bar{\mathbf{x}}_1, u) - f_{\text{ae}}(\bar{\mathbf{x}}_2, u)) \| \\
&\leq \|f_{\text{ae}}(\bar{\mathbf{x}}_1, u) - f_{\text{ae}}(\bar{\mathbf{x}}_2, u)\| \\
&\leq l\|\bar{\mathbf{x}}_1 - \bar{\mathbf{x}}_2\|.
\end{aligned} \tag{18}$$

From the Lipschitz assumption, the upper bound on the pitch angle error between its optimal nominal value and real value is derived in (19). The input for the optimal nominal state is u_0^* whereas the input for the real state is the disturbance compensated input u_c.

$$\|\bar{\alpha}^*(t|t_0) - \alpha(t)\|$$

$$= \|\bar{\alpha}^*(t_0) + \int_{t_0}^t \dot{\bar{\alpha}}^*(s)ds - \alpha(t_0) - \int_{t_0}^t \dot{\alpha}(s)ds\|$$

$$= \|\int_{t_0}^t \left(\int_{t_0}^s \ddot{\bar{\alpha}}^* \left(\bar{\mathbf{x}}^*(r|t_0), u_0^*(r|t_0)\right) dr\right) ds - \int_{t_0}^t \left(\int_{t_0}^s \ddot{\alpha}(\mathbf{x}(r), u_c(r|t_0))dr\right) ds\|$$

$$= \|\int_{t_0}^t \left(\int_{t_0}^s \ddot{\bar{\alpha}}^* \left(\bar{\mathbf{x}}^*(r|t_0), u_0^*(r|t_0)\right) dr\right) ds -$$

$$\int_{t_0}^t \left(\int_{t_0}^s \ddot{\alpha}(\mathbf{x}(r), u_0^*(r|t_0)) + \omega_{\text{res},\alpha}(r)dr\right) ds\| \tag{19}$$

$$\leq \int_{t_0}^t \left(\int_{t_0}^s \|\ddot{\bar{\alpha}}^*(\bar{\mathbf{x}}^*(r|t_0), u_0^*(r|t_0)) - \ddot{\alpha}(\mathbf{x}(r), u_0^*(r|t_0))\|dr + \bar{\omega}_m(s - t_0)\right) ds$$

$$\leq \int_{t_0}^t \left(\int_{t_0}^s l\|\bar{\mathbf{x}}^*(r|t_0) - \mathbf{x}(r)\|dr + \bar{\omega}_m(s - t_0)\right) ds$$

$$\leq \int_{t_0}^t \frac{\bar{\omega}_m}{l}(e^{l(s-t_0)} - 1)ds$$

$$= \frac{\bar{\omega}_m}{l^2}(e^{l(t-t_0)} - 1) - \frac{\bar{\omega}_m}{l}(t - t_0)$$

In (19), the last inequality comes from the Gronwall inequality. The maximum magnitude of $\omega_{\text{res},\alpha}$, represented by $\bar{\omega}_m$, can be either derived offline using (15) or online using (16).

The modified robust NMPC becomes

$$\mathbf{u}_{\text{opt}}(x) = \underset{u}{\operatorname{argmin}} \sum_{i=0}^{N-1} (||\bar{x}_i - x_{i,r}||_{Q_x} + ||u_i - u_{i,r}||_{Q_u}) + ||\bar{x}_N - x_{N,r}||_{Q_N}$$

$$\text{subject to } \dot{\bar{x}}(t) = f(\bar{x}(t)) + g(\bar{x}(t))u(\bar{x}(t)), \tag{20}$$

$$\bar{\alpha}_i \in [\min\{-5°, -20° + \mathcal{B}_\alpha(i)\}, \max\{5°, 20° - \mathcal{B}_\alpha(i)\}]$$

$$u_i \in [-10°, \ 10°]$$

where the augmented system dynamics with actuator and the aeroservoelastic models are implemented and the maximum state deviation, $\mathcal{B}_\alpha$, is defined by (21). A $\pm 5°$ margin is applied on the tightened constraints to prevent infeasible sets.

$$\mathcal{B}_\alpha(i) = \{\alpha \in \mathbb{R}^1 | \|\alpha\| \leq \frac{\bar{\omega}_m}{l^2}(e^{l\frac{T}{N}i} - 1) - \frac{\bar{\omega}_m}{l}(\frac{T}{N}i)\}, \tag{21}$$

Furthermore, because of the actuator dynamics, the command input β_c is decoupled from the disturbance. Therefore, disturbance compensation has to be applied to the real deflection. Instead of using the optimal command input u_0^*, the optimal flap deflection at the first step $\bar{\beta}_1^*$ is used as the reference signal. The disturbance compensated desired flap deflection is then defined as:

$$\beta_d = \begin{bmatrix} g_{\ddot{h}}(\mathbf{x}_f) \\ g_{\ddot{\alpha}}(\mathbf{x}_f) \end{bmatrix}^\dagger \left(\begin{bmatrix} g_{\ddot{h}}(\mathbf{x}_f) \\ g_{\ddot{\alpha}}(\mathbf{x}_f) \end{bmatrix} \bar{\beta}_1^* - \begin{bmatrix} \omega_h \\ \omega_\alpha \end{bmatrix}\right) \tag{22}$$

where disturbances ω_h and ω_α are estimated using (11).

A separate control law for the actuator is developed to track β_d while keeping the command input, u_c, inside the specified constraints.

$$u_c = u_0^* + \tanh(\frac{-k_u(\beta_f - \beta_d) + \beta_d - u_0^*}{\delta u}),\ k_u > 0 \tag{23}$$

$$\delta u = \begin{cases} 10^\circ - u_0^*, & \text{if } (-k_u(\beta_f - \beta_d) + \beta_d - u_0^*) \geq 0 \\ u_0^* + 10^\circ, & \text{otherwise.} \end{cases} \tag{24}$$

The control law described in (23) maintains the nominal performance of u_0^*, tracks the disturbance compensated desired deflection β_d, and keeps the command within the nominal constraint, but with a sacrificed disturbance rejection quality. The control gain k_u in (23) is set to four during simulation.

4.1 Simulation setup

In MATLAB 2023b environment, simulations are carried out to evaluate the performance of controllers for gust-induced LCO suppression tasks. The system dynamics are sampled at 1000 Hz, while the INDI controller operates at 100 Hz. The robust NMPC controller is tested with different controller sampling frequencies. The NMPC optimal control problem, described in (20), is formulated using the *nlmpcMultistage* controller object, with the optimal control action generated by the *nlmpcmove* command. Additionally, the prediction step N is set to 15, with a prediction horizon of 0.15 seconds. The input constraints are treated as hard constraints, while the state constraints are designed to be soft. Moreover, the states and input are scaled using the scaling matrix W_x and W_u. The specific values of W_x and weighting matrices Qx, Qu and Q_N can be found in Table 1.

The local Lipschitz constant l within the operation range is found to be 15, and the gust frequency is adopted from [19], setting to 2 Hz. The maximum gust is determined to be 4 m/s which gives the maximum pitch angle of 24.43 degrees, exceeding the nominal state constraints, from the open-loop simulation.

To demonstrate the conservativeness of the estimated upper bound on the state deviation in the robust NMPC, the NMPC controller is sampled at 6.67 Hz, such that the control horizon is equivalent to the prediction horizon, as illustrated in the inequality derived in (21). Furthermore, it is demonstrated that increasing the sampling frequency of the robust NMPC controller can mitigate the conservativeness of the tightened constraints. The subsequent simulations include assessing the effectiveness of INDI-coupled robust NMPC with offline identified worst possible disturbance $\bar{\omega}_m$. Finally, the proposed INDI-based online estimation of maximum state deviation with INDI-coupled robust NMPC is simulated to demonstrate the further reduction of the conservativeness of the tightened constraints.

Table 1: Controller parameters in the robust NMPC

Parameter	Description	Value
W_x	Stae scaling factor	diag($\begin{bmatrix} 0.0279 & 0.4894 & 0.4952 & 6.8143 & 0.3491 \end{bmatrix}$
W_u	Input scaling factor	0.3491
Q_x	State weight	diag($\begin{bmatrix} 1 & 10 & 0 & 0 & 0 \end{bmatrix}$
Q_u	Input weight	0.1
Q_N	Terminal weight	diag($\begin{bmatrix} 15 & 150 & 0 & 0 & 0 \end{bmatrix}$

5 RESULTS

5.1 Simulation for nominal NMPC with controller frequency of 6.67 Hz

The conservativeness of the robust NMPC with tightened constraints is first examined. The NMPC configurations adhere to the precise mathematical formulations specified in (21), where the control horizon matches the prediction horizon. To determine the minimal value of the parameter $\bar{\omega}_m$ as per (21), a series of NMPC simulations were performed under different gust disturbances. This parameter, once estimated offline, effectively bounds the pitch angle deviation using (21) and is subsequently used to tighten the pitch angle state constraints in the robust NMPC scheme.
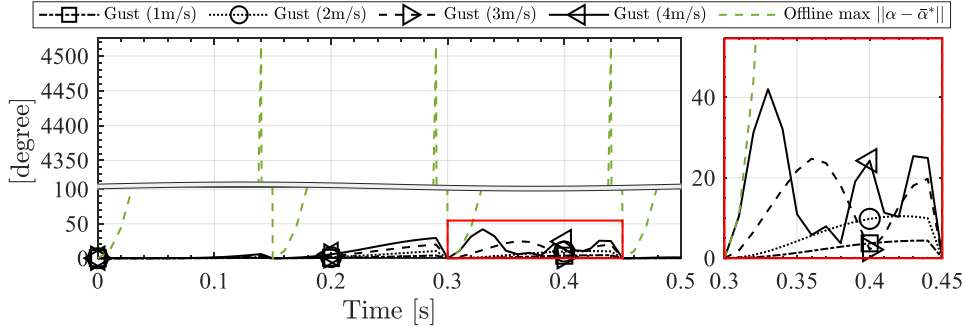
Figure 1: Offline estimation on the upper bound of the additive disturbances. A separate zoomed in plot on the right shows that state deviations are bounded by (21) with $\bar{\omega}_m = 3500$ rad/s^2.

Deviations between the actual and predicted optimal pitch state trajectories under four gust conditions are depicted in Figure 1. The largest deviation occurs between 0.3 seconds and 0.45 seconds due to a 4 m/s 1-cos discrete-time gust. A detailed examination in the zoomed-in plot reveals that these angle deviations across all cases are norm bounded by (21) with $\bar{\omega}_m$ at 3500 rad/s^2, indicated by the dashed green line.

However, this estimated value of $\bar{\omega}_m$ from (21) results in a worst-case pitch angle deviation of 10.55 degrees at the first prediction step. Therefore, a conservative tightened constraint of ± 9.45 degrees is derived. More critically, the worst deviations beyond the first prediction step are larger than 44.44 degrees, exceeding the nominal constraint limit of ± 20 degrees and consequently leading to infeasible tightened constraint sets. Such conservative and even infeasible tightened constraints could render the optimal control problem unsolvable. Fortunately, fast sampling NMPC controllers, with one control horizon, have mitigated the conservativeness of the robust NMPC.

5.2 Simulation for nominal NMPC with controller frequency of 100 Hz

The conservativeness of the robust NMPC with tightened constraints often leads to mathematically infeasible problems. This issue can be alleviated by using the NMPC scheme with a faster controller frequency. In this simulation, the controller frequency is increased from 6.67 Hz to 100 Hz, reducing the control horizon from fifteen to one.

As highlighted previously, the maximum state deviation occurred under the largest gust condition of 4 m/s. Accordingly, later simulations focus exclusively on 4 m/s gust case. From the NMPC simulation with a control horizon of one, the minimal value of $\bar{\omega}_m$ is 1200 rad/s^2, which is 65.71% smaller than the case where control horizon equals the prediction horizon. In Figure 2, the top plot displays the trajectories of disturbed pitch angles and the optimal nominal

pitch angle. In the bottom plot, the offline estimated worst deviation of α with $\bar{\omega}_m$ of 1200 rad/s^2 upper bounds the real deviation.
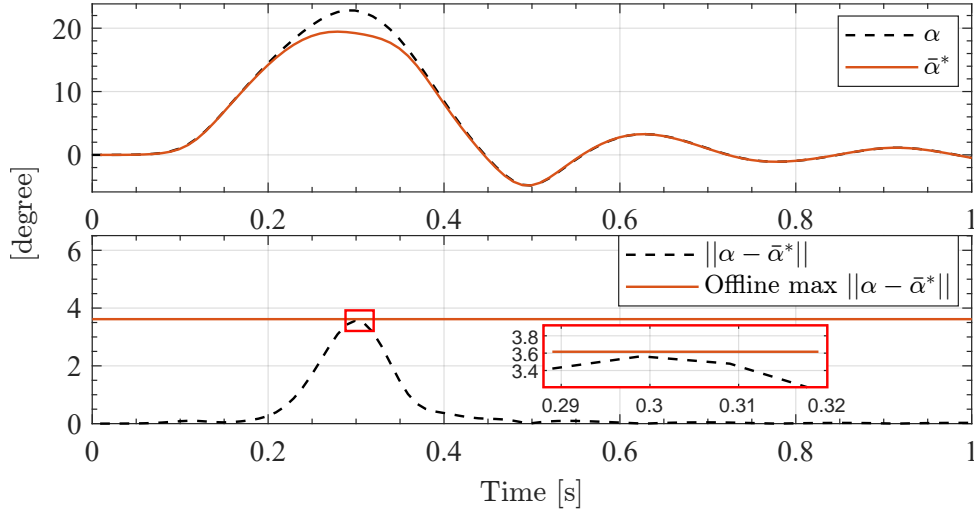

Figure 2: Simulation results of nominal NMPC with 100 Hz controller frequency. The top plot includes optimal nominal and real pitch angle trajectories. The bottom plot includes the pitch angle deviation due to the gust and the upper bound of this deviation using (21).

Despite the reduction in $\bar{\omega}_m$, Equation 21 gives the worst pitch angle deviation of 15.24 degrees at the second prediction step, resulting in a conservative tightened constraint of ± 4.76 degrees. Unfortunately, tightened constraints after the second step also fall into infeasible sets, as the predicted worst deviations exceed the nominal constraints. These new tightened constraints, although relatively more relaxed than in previous simulations, again underscore the conservativeness of robust NMPC when tightened constraints are used.

5.3 Simulations for nominal NMPC, robust NMPC and INDI-coupled robust NMPC ($\bar{\omega}_m = 1200 \; rad/s^2$)

In this section, the robust NMPC and INDI-coupled robust NMPC are simulated with the 4m/s gust, with $\bar{\omega}_m$ of 1260 rad/s^2 derived from the previous section, and with the ± 5 degrees margin on the pitch angle tightened constraint. Moreover, the results from these two robust control schemes are compared with the open-loop response and the NMPC simulation results.

First, the open-loop state phase portraits with zero initial states are plotted in Figure 3, showing the 4 m/s 1-cos discrete-time gust-induced LCOs in the plunge and pitch motions. The phase portraits from the INDI-coupled robust NMPC closed-loop response are plotted alongside the open-loop response, showing the elimination of gust-induced LCOs. Figure 4 compares the plunge and pitch motions of the wing section. All three methods stabilize the systems which otherwise experience gust-induced LCOs in the open-loop response. For the plunge movement, there are -17.14%, 11.23% and 20.69% peak reductions using NMPC, robust NMPC and INDI-coupled robust NMPC. In addition, The peak pitch angles are reduced by 6.54%, 19.72% and 33.70% for these three methods, respectively. The maximum pitch angle from the robust NMPC simulation is within the nominal constraint, which demonstrates the robustness of the tightened constraint procedure. Furthermore, the superior performance of INDI-coupled robust NMPC shows the success of using INDI to reject disturbances.

Figure 5 contains visualizations of the tightened constraint procedure for robust NMPC and INDI-coupled robust NMPC. The peak value of α (red line) may intersect with the tightened

constraint, implying the violation of the soft constraint. As a result, the reachability question arises. Will the system return to the feasible region in one step? This will be a future research topic investigating the reachability control problem. Currently, the introduction of slack variables from the soft constraints partially addresses this problem. In addition, in Figure 5 (b),
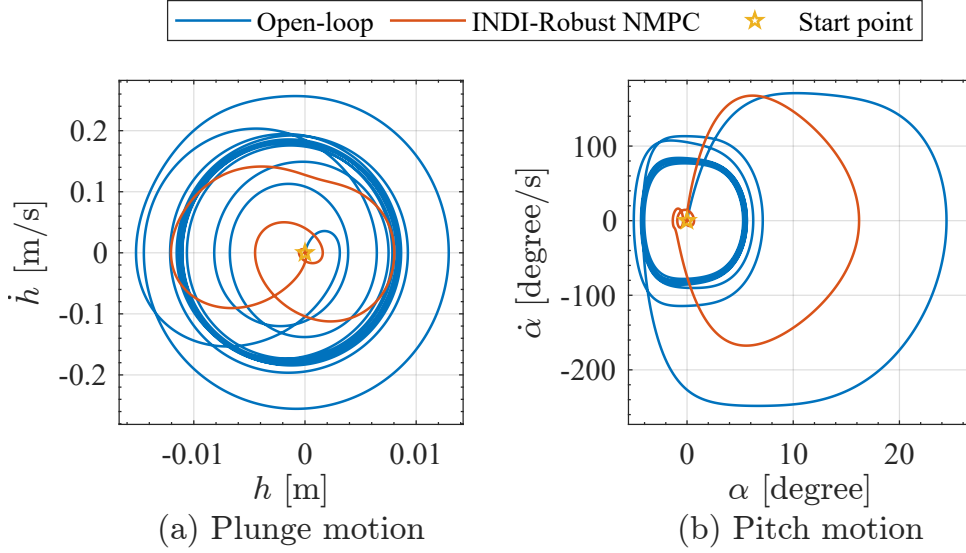

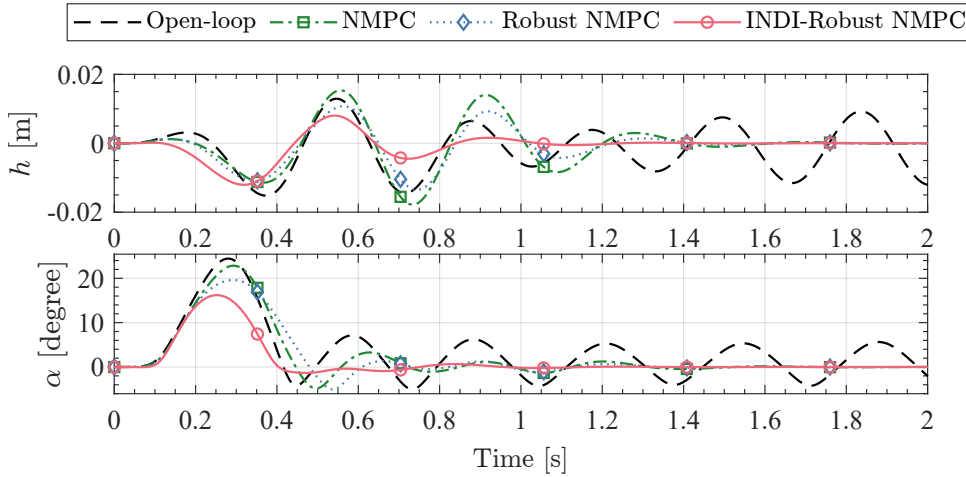Figure 3: Phase portraits from the open-loop gust response and INDI-robust NMPC closed-loop gust response.

Figure 4: Open-loop gust response and closed-loop results using NMPC, robust NMPC, and INDI-robust NMPC.
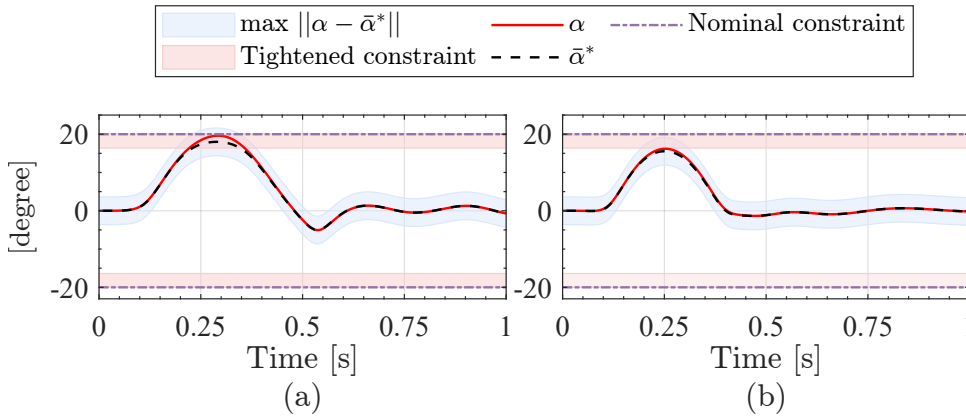
Figure 5: Visualization of the tightened constraints procedure. (a) Robust NMPC. (b) INDI-robust NMPC.

there exist large margins between the real trajectory and the possible state deviation represented by the blue area, indicating that INDI can further reduce the value of $\bar{\omega}_m$. In the next section, we show that the INDI-based sliding window online estimation of maximum deviation can further mitigate the conservativeness of the tightened constraint.

5.4 INDI-coupled robust NMPC with an online estimation of $\bar{\omega}_m$

It has been shown in (14) and observed from Figure 5 (b) that the INDI-coupled robust NMPC has the potential to further reduce the magnitude of $\bar{\omega}_m$ for a more relaxed tightened constraint. By using the proposed INDI-based online estimation from (16), we demonstrate the power of online estimation to reduce the conservativeness of tightened constraint and potentially eliminate the reachability concern.
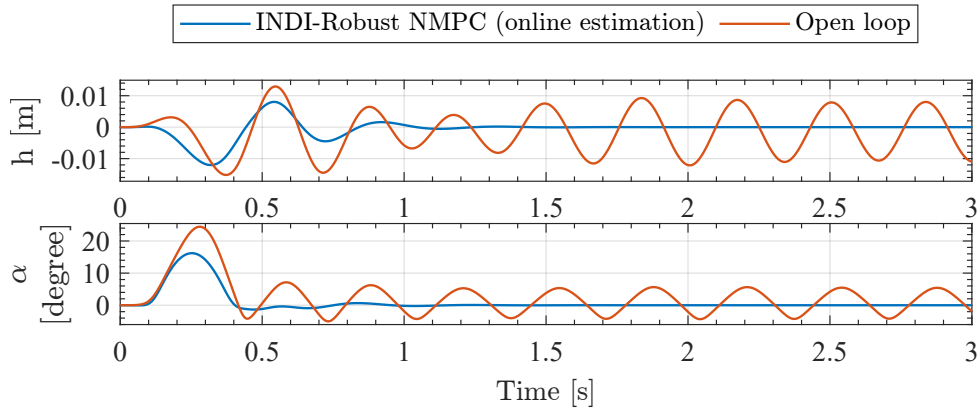

Figure 6: Open-loop gust response and closed-loop results using INDI-robust NMPC with online estimation of $\bar{\omega}_m$.

Firstly, Figure 6 shows simulation results of the INDI-coupled robust NMPC with online disturbance parameter estimation. The sliding window size is 0.15 seconds, which equals the prediction horizon. The proposed online estimation robust control method achieves the same peak reductions of 20.69% and 33.70% in the plunge and pitch motions compared to the results from the INDI-coupled robust NMPC with the offline identified $\bar{\omega}_m$.
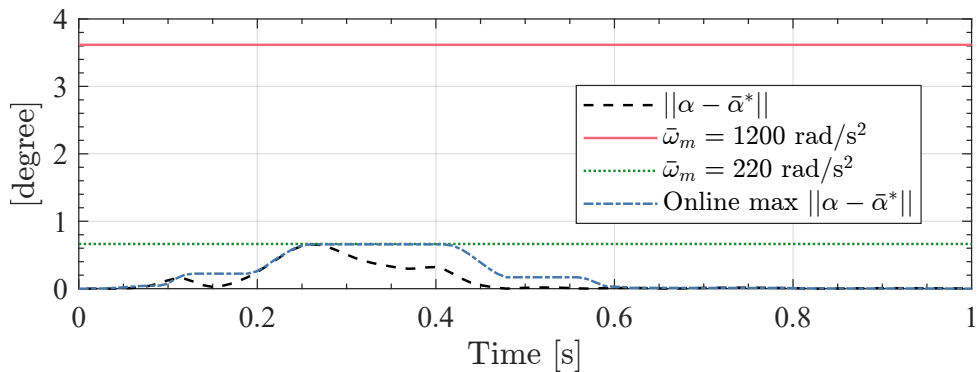

Figure 7: Pitch angle errors and estimated maximum pitch angle errors between optimal nominal and real values. Errors are estimated using the offline identified maximum disturbance, the offline identified maximum disturbacne residue, and the online sliding window maximum disturbance residue.

The significant takeaway for this online INDI-coupled robust NMPC is the relaxation of the parameter $\bar{\omega}_m$. In Figure 7, we have plotted pitch angle deviation with the black dashed line from the proposed method (online estimation). The red line represents (21) for the first prediction step with $\bar{\omega}_m = 1200$ rad/s^2, the nominal disturbance upperbound. The green dotted line is

the offline estimation of minimal disturbance residue using (21) that upper bounds the state deviation, with the minimal value being 220 rad/s^2. Therefore, with the integration of INDI in robust NMPC, the conservativeness is further reduced, and in our case, the tightened constraint can be relaxed by 81.67%.

Furthermore, looking at the shape of the online estimated maximum state deviation represented by the blue dash-dot line, we find that the INDI-based online estimation successfully captures the maximum real deviation. There are few time instances when the estimated deviation is smaller than the real one. However, these instances happen when the real deviations are small, and therefore, does not influence the robustness of overall performances. Overall, the online estimation further relaxes the tightened constraint compared to the offline estimation of $\bar{\omega}_m$ when the real state deviations are small. Not only is the conservativeness of tightened constraint further mitigated by the online estimation, but the reachability problem is also resolved in our study case. In Figure 8, the real trajectory does not exceed the tightened constraints, indicating that there exist a feasible set for the state to steer to in the next step.
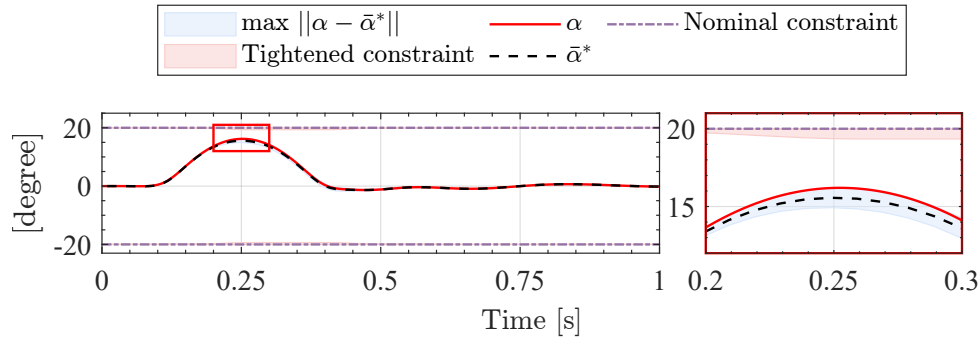

Figure 8: Visualization of the tightened constraints from INDI-robust NMPC with online state error estimation.

6 CONCLUSION

In this study, we developed and evaluated a novel INDI-coupled robust NMPC framework for gust-induced LCO suppression tasks. Integrating INDI with robust NMPC allowed for effective disturbance rejection and reduced conservativeness of the tightened constraints. Simulation results using a 2-D nonlinear aeroservoelastic wing under the worst gust condition demonstrated that the proposed approach stabilized the system and achieved significant reductions in peak plunge and pitch motions compared to traditional NMPC and robust NMPC methods. Specifically, the online INDI-based estimation of maximum state deviation further relaxed the tightened constraints, enhancing the feasibility of the control scheme. Future work will focus on analyzing the reachability of the system when states start outside of the tightened constraints.

7 REFERENCES

[1] Zhang, K., Shi, Y., and Sheng, H. (2021). Robust nonlinear model predictive control based visual servoing of quadrotor uavs. *IEEE/ASME Transactions on Mechatronics*, 26(2), 700–708. doi:10.1109/TMECH.2021.3053267.

[2] Patil, M. J. and Hodges, D. H. (2002). Output feedback control of the nonlinear aeroelastic response of a slender wing. *Journal of Guidance, Control and Dynamics*, 25, 302–308.

[3] Fazelzadeh, S. A. and Jafari, S. M. (2008). Active control law design for flutter suppression and gust alleviation of a panel with piezoelectric actuators. *Smart Materials and Structures*, 17. ISSN 09641726. doi:10.1088/0964-1726/17/3/035013.

13

[4] Liu, X., Sun, Q., and Cooper, J. E. (2017). Lqg based model predictive control for gust load alleviation. *Aerospace Science and Technology*, 71, 499–509. ISSN 12709638. doi: 10.1016/j.ast.2017.10.006.

[5] Liu, X. and Sun, Q. (2017). Improved lqg method for active gust load alleviation. *Journal of Aerospace Engineering*, 30. ISSN 0893-1321. doi:10.1061/(asce)as.1943-5525. 0000712.

[6] Duessler, S., Mylvaganam, T., and Palacios, R. (2023). Lqg-based gust load alleviation systems for very flexible aircraft. American Institute of Aeronautics and Astronautics (AIAA). doi:10.2514/6.2023-2571.

[7] Duessler, S., Mylvaganam, T., and Palacios, R. (2024). Modelling for design and performance evaluation of gust load alleviation systems for flexible aircraft. American Institute of Aeronautics and Astronautics. ISBN 978-1-62410-711-5. doi:10.2514/6.2024-0614.

[8] Forte, C. J. and Nguyen, N. T. (2024). Multi-objective optimal control of high aspect ratio wing wind tunnel model. American Institute of Aeronautics and Astronautics. ISBN 978-1-62410-711-5. doi:10.2514/6.2024-1782.

[9] Fournier, H., Massioni, P., Pham, M. T., et al. (2022). Robust gust load alleviation of flexible aircraft equipped with lidar. *Journal of Guidance, Control, and Dynamics*, 45, 58–72. ISSN 15333884. doi:10.2514/1.G006084.

[10] Ting, K. Y., Mesbahi, M., Livne, E., et al. (2022). Wind tunnel study of preview h2 and h control for gust load alleviation of flexible aircraft. American Institute of Aeronautics and Astronautics Inc, AIAA. ISBN 9781624106316. doi:10.2514/6.2022-2489.

[11] de Souza, A. D. R., Vuillemin, P., Poussot-Vassal, C., et al. (2023). Gust load alleviation using reduced-order aeroelastic models and observer-based robust control. doi:10.2514/1. G007153.

[12] Prime, Z., Cazzolato, B., and Doolan, C. *Mixed H2/Hinf Scheduling Control Scheme for a Two Degree-of-Freedom Aeroelastic System Under Varying Airspeed and Gust Conditions*. doi:10.2514/6.2008-6787.

[13] Barker, J. M. and Balas, G. J. (2000). Comparing linear parameter-varying gain-scheduled control techniques for active flutter suppression. *Journal of Guidance, Control, and Dynamics*, 23(5), 948–955. doi:10.2514/2.4637.

[14] Wang, X., Kampen, E. V., Chu, Q. P., et al. (2019). Flexible aircraft gust load alleviation with incremental nonlinear dynamic inversion. *Journal of Guidance, Control, and Dynamics*, 42, 1519–1536. ISSN 15333884. doi:10.2514/1.G003980.

[15] Wang, X., Mkhoyan, T., Mkhoyan, I., et al. (2021). Seamless active morphing wing simultaneous gust and maneuver load alleviation. *Journal of Guidance, Control, and Dynamics*, 44, 1649–1662. ISSN 15333884. doi:10.2514/1.G005870.

[16] Artola, M., Goizueta, N., Wynn, A., et al. (2021). Aeroelastic control and estimation with a minimal nonlinear modal description. *AIAA Journal*, 59, 2697–2713. ISSN 1533385X. doi:10.2514/1.J060018.

[17] Artola, M., Wynn, A., and Palacios, R. (2022). Modal-based nonlinear model predictive control for 3-d very flexible structures. *IEEE Transactions on Automatic Control*, 67, 2145–2160. ISSN 15582523. doi:10.1109/TAC.2021.3071326.

[18] Wynn, A., Artola, M., and Palacios, R. (2022). Nonlinear optimal control for gust load alleviation with a physics-constrained data-driven internal model. American Institute of Aeronautics and Astronautics Inc, AIAA. ISBN 9781624106316. doi:10.2514/6.2022-0442.

[19] Sun, B., Wang, X., and van Kampen, E. J. (2022). Event-triggered intelligent critic control with input constraints applied to a nonlinear aeroelastic system. *Aerospace Science and Technology*, 120. ISSN 12709638. doi:10.1016/j.ast.2021.107279.

[20] Haughn, K. P. T., Harvey, C., and Inman, D. J. (2024). Deep learning reduces sensor requirements for gust rejection on a small uncrewed aerial vehicle morphing wing. *Communications Engineering*, 3, 53. ISSN 2731-3395. doi:10.1038/s44172-024-00201-8.

[21] Nguyen, N. T. and Tuzcu, I. (2024). Nonlinear distributed hamiltonian control of very flexible aircraft with adaptive gust rejection. American Institute of Aeronautics and Astronautics. ISBN 978-1-62410-711-5. doi:10.2514/6.2024-1784.

[22] Rubagotti, M., Raimondo, D. M., Ferrara, A., et al. (2011). Robust model predictive control with integral sliding mode in continuous-time sampled-data nonlinear systems. *IEEE Transactions on Automatic Control*, 56(3), 556–570. doi:10.1109/TAC.2010.2074590.

[23] Xie, H., Dai, L., Lu, Y., et al. (2022). Disturbance rejection mpc framework for input-affine nonlinear systems. *IEEE Transactions on Automatic Control*, 67(12), 6595–6610. doi:10.1109/TAC.2021.3133376.

[24] Sun, S., Romero, A., Foehn, P., et al. (2022). A comparative study of nonlinear mpc and differential-flatness-based control for quadrotor agile flight. *IEEE Transactions on Robotics*, 38(6), 3357–3373. doi:10.1109/TRO.2022.3177279.

COPYRIGHT STATEMENT